Chalcogenide Letters Vol. 17, No. 4, April 2020, p. 197 - 205

# POLYLOL S0LUTION SYNTHESIS OF ORIENTED $In_2Se_3$ NANOSHEETS AND THEIR APPLICATION ON HIGH-PERFORMANCE INORGANIC-ORGANIC HYBRID PHOTODETECTOR

Y. L. MA[a,*], X. L. CHEN[a], J. WANG[b], X. HUANG[b], H. M. JI[b], Z. G. JIN[b]
[a]*College of Physics and Electronic Information Engineering, Qinghai University for Nationalities, Xining 810007, China*
[b]*Key Laboratory of Advanced Ceramics and Machining Technology of Ministry of Education, School of Materials Science and Engineering, Tianjin University, Tianjin 300072, China*

Single-phase β-$In_2Se_3$ nanosheets were successfully synthesized by hot injection method using triethylene glycol (TEG)-based solution. It was found that the adding amounts of reactant played a key role in determining size and thickness of the $In_2Se_3$ nanosheets. The $In_2Se_3$ nanosheets were (0001) orientation and had the lateral size of ~500 nm and plate thickness of ~6 nm with 0.4 mmol indium precursor. A new inorganic-organic hybrid film photodetector using the oriented $In_2Se_3$ nanosheets and photoelectronic Poly(3-hexylthiophene) (P3HT) as blending partners was fabricated on $SiO_2$/Si wafer, exhibiting a much better photoswitching performance with a low off-current of ~40 pA at a bias voltage of 1.0 V and on/off ratio of 250 illuminated at 532 nm under incident light intensity of 40 mW/cm$^2$.

(Received January 19, 2020; Accepted April 9, 2020)

*Keywords:* $In_2Se_3$ nanosheets, Solution process, P3HT, Hybrid photodetector

## 1. Introduction

Electrons are limited in two-dimensional (2D) structure, which makes 2D layered materials have excellent physical and chemical properties [1,2]. In recent years, 2D structures such as grapheme [3], phosphorene [4] and $MoS_2$ [5] have been studied continuously as novel and promising materials. Similar to the materials mentioned above, $In_2Se_3$ has a layered structure, which is connected by Se-In in the layer, and is stable by weak van der Waals force between layers [6-8]. In addition, $In_2Se_3$ exhibits the advantages of adjustable bandgap [9], spontaneous polarization [10] and suppression of photo-carrier combination [11], making it fashionable in the fields of optoelectronic devices [12-14], lithium-ion batteries [15], phase change materials [16], catalysts [17] and so on. At present, high quality $In_2Se_3$ nanosheets usually were prepared by vapor phase method [13,14,18,19] and exfoliation technique [20]. However, $In_2Se_3$ has complex crystal structures (α, β, γ, δ, κ) [19,21] and Indium can be easily hydrolyzed [22], resulting in difficulty in fabricating a single phase, especially 2D layered $In_2Se_3$, by a solution method.

Here, we obtained the pure β-$In_2Se_3$ nanosheets with only a few molecular layers by simple hot injection method, which avoids the shortcomings of using oleylamine [23] and a long

*Corresponding author: myl2005114@163.com

solvothermal process [24]. This simple solvent method not only obtains high-quality nanosheets with good dispersibility, but also has low cost and is easy to mass-produce. P3HT, widely used in polymer solar cells, has high electronic conductivity and a wider band gap, which limits its absorption of long wavelength light [25]. The combination of P3HT and selenide with broad spectrum absorption and high carrier mobility into inorganic-organic hybrid devices can provide exciting photoelectric characteristics [26]. In view of this, the β-$In_2Se_3$ nanosheets and P3HT are mixed to prepare high performance photodetectors, which broadens the application of $In_2Se_3$ in the field of photodetectors.

## 2. Experimental

### 2.1. Synthesis of $In_2Se_3$ Nanosheets (NSs)

In present work, 0.2 mmol $InCl_3 \cdot 4H_2O$ was dissolved into 10 mL of TEG as Indium precursor solution. 0.3 mmol Se, 0.2000 g PVP and 50 μL $N_2H_4 \cdot H_2O$ were poured into 40 mL of TEG solvent in a three-necked flask as Se precursor solution. The flask was heated to the solution temperature of 270 ℃ where the indium precursor was slowly dripped at a rate of 1 mL/min. The solution was refluxed at 270 ℃ for 30 min. The $In_2Se_3$ nanosheets, marked as S1, were extracted by high speed centrifugation and then were purified by absolute ethanol. In another synthesis of larger $In_2Se_3$ nanosheets, the adding amounts of $InCl_3 \cdot 4H_2O$, Se powder, PVP and $N_2H_4 \cdot H_2O$ were 0.4 mmol, 0.6 mmol, 0.4000 g, 100 μL, respectively. The other processing parameters were kept the same as those in the synthesis above. These products were marked as S2.

### 2.2. Fabrication of photodetector devices

Comb-like Au pair electrodes were fabricated on clear $SiO_2$/Si substrates. The gap distance between the electrode wirings was 2 μm. The 1, 2-dichlorobenzene solution of $In_2Se_3$ nanosheets (30 mg/mL) was coated on the $SiO_2$/Si substrates by blade-coating method to prepare $In_2Se_3$ photodetector devices. Then the 200 μL 1, 2-dichlorobenzene solution of S2 sample (30 mg/mL) was mixed with 100 μL P3HT solution (15 mg/mL) to prepare $In_2Se_3$/P3HT hybrid photodetector devices.

### 2.3. Materials characterization

The products were characterized by X-ray diffraction (XRD, D8 advanced, Bruker, Germany) with CuKα radiation (λ=1.5418 Å), scanning electron microscopy (SEM, S-4800, Hitachi, Japan), high-resolution transmission electron microscopy (HRTEM, Tecnai G2 F20, FEI, Netherlands). Raman spectra were recorded between 100 $cm^{-1}$ and 400 $cm^{-1}$ by a micro-Raman instrument (HR800, HORIBA Scientific) with excitation laser line at 514 nm. UV-Vis–NIR spectra at wavelength from 400 nm to 1500 nm were collected with a UV-Vis–NIR spectrophotometer (UV-3600, Shimadzu, Japan). The thickness of $In_2Se_3$ nanosheets was measured by a Multimode nanoscope IV atomic force microscope (AFM, 5500, Agilent, USA). I–V characteristics of the devices were measured at room temperature in air with a Keithley 2400 digital sourcemeter (USA) both in a dark chamber and under illumination at 100 $mW/cm^2$ using an AM 1.5 solar simulator (XES-40S1, SAN-EI Electric, Japan). Monochromatic light from a laser (STONE Laser, China) was focused onto the films.

## 3. Results and discussion

Fig. 1shows that all diffraction peaks of the XRD patterns can be indexed to the standard pattern of rhombohedral β-$In_2Se_3$ (JCPDS Card No. 35-1056, space group $R\bar{3}m$), suggesting that the change of reactant concentration did not affect crystallized phase. The diffraction peak (006) of the XRD pattern has an obvious preferential strengthening compared with the standard pattern, which is associated with its growing morphology by TEM observation mentioned below.

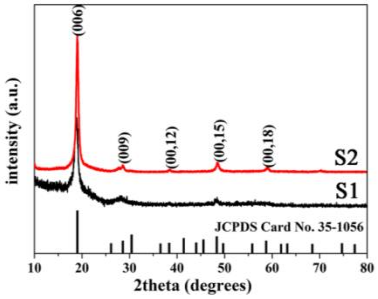


*Fig. 1. XRD pattern of the S1 and S2*

Fig. 2 is the Raman spectrum of S1 and S2 within the range from 100 $cm^{-1}$ to 400 $cm^{-1}$. The peaks at 108 $cm^{-1}$ and 206 $cm^{-1}$ are attributed to $A_{1g}^1$ and $A_{1g}^2$ modes, respectively [27], and the 255 $cm^{-1}$ vibration mode originates from the $Se_8$ rings [28]. The small change to lower wavenumbers, with the decreasing of thickness, is consistent with a recent report [29].

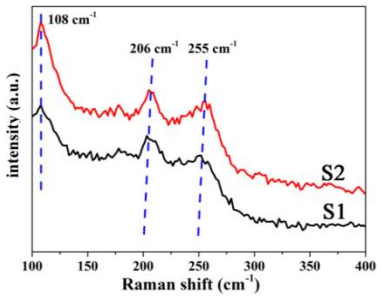


*Fig. 2. Raman spectrum of the S1 and S2*

Shown in Fig. 3(b, c, e, f), the lateral size of the hexagonal $In_2Se_3$ NSs significantly increases with a doubling of reagent concentration, but the interplanar distance of samples S1 and S2 are both 0.342 nm for the (101) plane of $In_2Se_3$. The selected area electron diffraction (SAED) pattern with incident electron beam perpendicular to the plate-surface shows single-crystalline diffraction spots, demonstrating that the surface of $In_2Se_3$ NSs are both [0001] orientation. Fig. 3a shows the Se-In-Se-In-Se quintuple layer (QL) is attached to each other through weak van der Waals forces, in which In atoms are located in octahedral cages formed by Se packing and each QL is 1 nm thickness [16]. The thickness of the $In_2Se_3$ NSs was determined by AFM (Fig. 3(d, g)). The average thickness of S1 and S2 is ~2.3 nm (~2 QLs) and ~5.4 nm (~5 QLs), respectively, indicating an effective increase of the thickness with reagent concentration. The increase in lateral size and thickness is due to enhance the driving forces of the chemical synthesis in the stage of explosive nucleation and following growth [30].

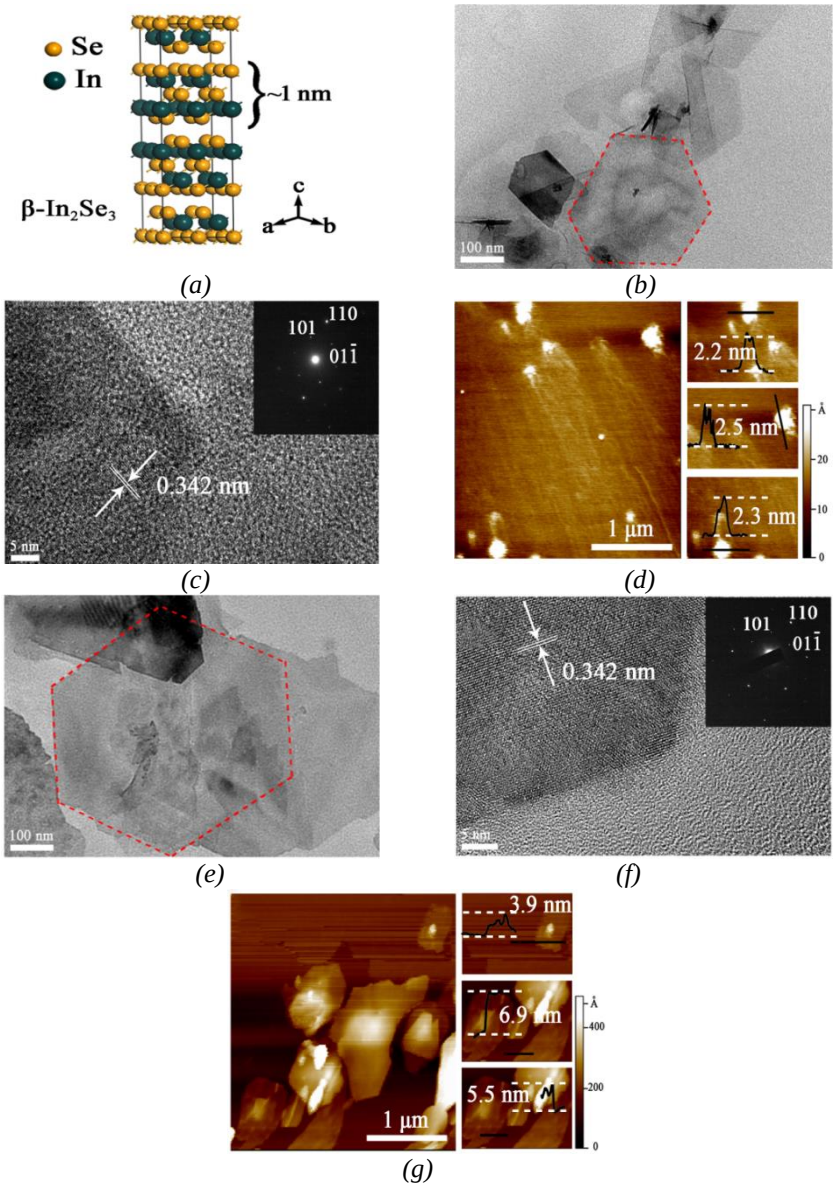


*Fig. 3. (a) Schematic crystal structure of rhombohedral β-$In_2Se_3$. TEM images and AFM analysis of (b,c,d)S1 and (e,f,g)S2. The insets are SAED patterns.*

The direct band gap of S1 and S2 was determined to be 1.91 eV and 1.76 eV, respectively, by the Kubelka-Munk function [31], as depicted in Fig. 4. The direct band gap energy has blue shift by 0.61 eV for S1 and 0.46 for S2 to bulk $In_2Se_3$ (1.30 eV) because of the quantum confinement effect [6]. The optical band gap is influenced by the thickness of $In_2Se_3$ NSs, increasing from 1.76 eV for S2 sample of ~5.4 nm thickness to 1.91eV for S1 sample of ~2.3 nm thickness. The $In_2Se_3$ photodetector devices were fabricated on the $SiO_2$/Si substrates with comb-like pair Au electrode, as shown in Fig. 5(a-b).

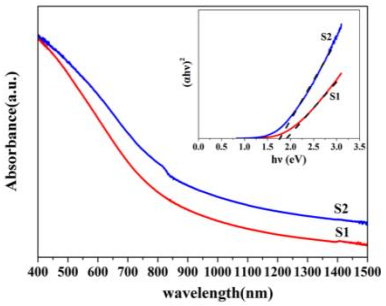


*Fig. 4. UV-Vis-NIR spectroscopic characterization of S1 and S2.*

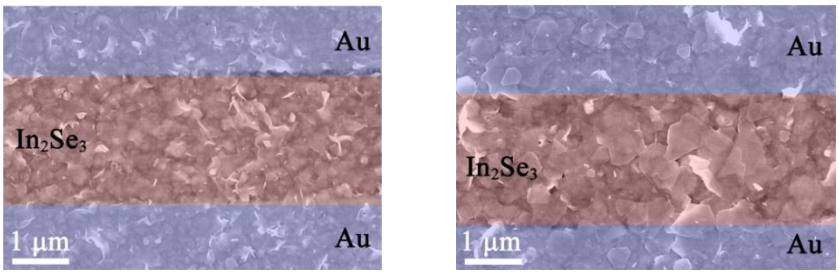


*Fig. 5. False-colored SEM images of a typical $In_2Se_3$ photodetector by (a)S1 and (b)S2.*

Fig. 6(a-f) shows that I–V characteristics and transient photocurrent of the $In_2Se_3$ NSs photodetector were measured in the dark condition and under illumination. In the dark, the bias current of S1-photodetector and S2-photodetector were 0.66 nA and 0.41 nA, respectively. At incident light intensity of 100 $mW/cm^2$ and bias voltage of 1.0 V, the current response of S1-photodetector and S2-photodetector could reach 5.8 nA and 8.6 nA, showing the on/off ratio of ~9 and ~20, respectively. Meanwhile, To ascertain further the feasibility of, S1-photodetector and S2-photodetector were illuminated under different lights across wavelengths of 405 nm to 1064 nm, with a fixed light intensity of 40 $mW \cdot cm^{-2}$ at a bias voltage of 1 V. For wavelength of 532 nm, the maximum values of photocurrent are achieved in both photodetectors, showing 13.4 nA for S1-photodetector and 24.8 nA for S2-photodetector. For wavelength of 1064 nm, the photocurrent is still detectable but very weak.

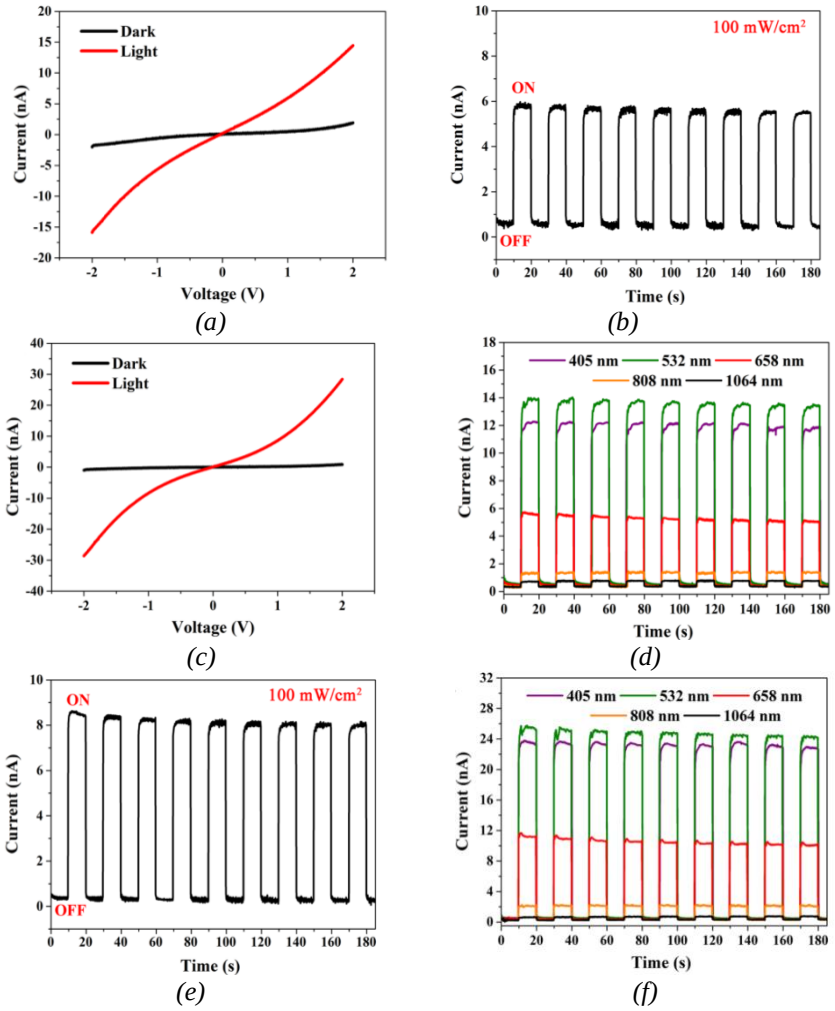


*Fig. 6. I–V characteristics and Transient photocurrent of the (a,b)S1 and (c,d)S2. Transient photocurrent of the (e)S1 and (f)S2.*

Fig. 7. shows the $In_2Se_3$-P3HT hybrid photodetector device which were prepared by $In_2Se_3$ NSs (S2 sample) and P3HT. In $In_2Se_3$-P3HT hybrid photodetector, the top of the valence band of β-$In_2Se_3$, which corresponds the HOMO of -5.2 eV for P3HT, is -6.27 eV [32]. Based on the direct band-gap structure, the bottom of the conduction band, which corresponds to the LUMO of -3.2 eV for P3HT, is calculated to be -4.37 eV, which indicate the band-structure match between $In_2Se_3$ NSs and P3HT and will contribute significantly to the photogenerated carriers dissociation at the interface.

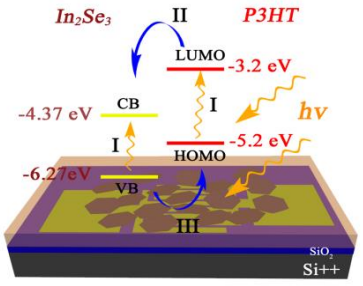


*Fig. 7. The energy level diagram and device structure of $In_2Se_3$-P3HT blend.*

In the dark, the device was nearly insulating, and the bias current was only 40 pA, which suggests an remarkable cut-off capability and low noise.At incident light intensity of 100 mW/cm$^2$ and bias voltage of 1.0 V, the current response could reach 4.3 nA, showing an on/off ratio of ~100. Similarly, shown in Figure 8(a), the maximum value of photocurrent are achieved at wavelength of 532 nm and intensity of 40 mW·cm$^{-2}$. The $In_2Se_3$/P3HT hybrid photodetector have much better photoswitching performance with a low off-current of ~40 pA at bias voltage 1.0 V and on/off ratio of 250. In contrast, the pure $In_2Se_3$ NSs photodetector had only low on/off ratio (~60) and high dark current (~410 pA) because of the hardness to dissociate efficiently into electrons and holes in the absence of the hole acceptor. In the $In_2Se_3$ NSs-P3HT hybrid structure, the electron-hole pairs are photogenerated under illumination, in which the $In_2Se_3$ NSs can act as a photoelectron acceptor, and P3HT is perfect for acting as a hole acceptor. In conclusion, the $In_2Se_3$/P3HT hybrid photodetector exhibits a better photoresponse performance and can be applied to serve as a high-quality photosensitive switch.

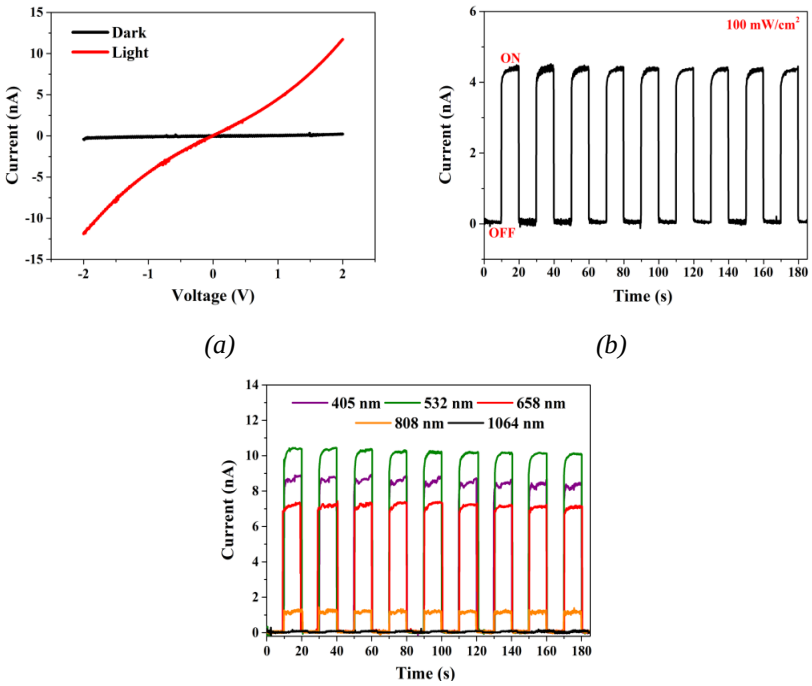


*(a)* *(b)*

*(c)*

*Fig. 8. (a) I-V characteristics and (b) transient photocurrent of the $In_2Se_3$/P3HT hybrid photodetector (c) Transient photocurrent of the $In_2Se_3$/P3HT hybrid photodetector.*

## 4. Conclusions

Single-phase and (0001)-oriented β-$In_2Se_3$ nanosheets were successfully synthesized by the atmospheric pressure hot injection method. The thickness of $In_2Se_3$ nanosheets increased from 2.3 nm to 5.4 nm by doubling the concentration of raw materials. A new inorganic-organic hybrid film photodetector was fabricated on $SiO_2$/Si wafer, exhibiting a much better photoswitching performance with low off-current of ~40 pA and high on/off ratio of 250. Its switching in two states was fast, high sensitive, low noise and reversible, allowing the device to serve as a

promising high-quality photosensitive switch.

**Acknowledgements**

The authors acknowledge the financial support from Key Natural Science Foundation of Qinghai province (2017-zj-729).

## References

[1] Y. Guo, K. Xu, C. Wu, J. Zhao, Y. Xie, Chem. Soc. Rev. **44**(3), 637 (2015).
[2] H. Zhang, ACS nano. **9**(10), 9451 (2015).
[3] C. Yan, J. Wang, W. Kang, M. Cui, X. Wang, C. Y. Foo, K. J. Chee, P. S. Lee, Adv. Mater. **26**(13), 2022 (2014).
[4] M. Batmunkh, M. Bat-Erdene, J. G. Shapter, Adv. Mater. **28**(39), 8586 (2016).
[5] T. Wang, J. Li, G. Zhao, Powder Technology. **253**, 347 (2014).
[6] G. Almeida, S. Dogan, G. Bertoni, C. Giannini, R. Gaspari, S. Perissinotto, R. Krahne, S. Ghosh, L. Manna, J. Am. Chem. Soc. **139**(8), 3005 (2017).
[7] T. Zhai, Y. Ma, L. Li, X. Fang, M. Liao, Y. Koide, J. Yao, Y. Bando, D. Golberg, J. Mater. Chem. **20**(32), 6630 (2010).
[8] W. Ding, J. Zhu, Z. Wang, Y. Gao, D. Xiao, Y. Gu, Z. Zhang, W. Zhu, Nat. Commun. **8,** 14956 (2017).
[9] H. Bouzouita, N. Bouguila, S. Duchemin, S. Fiechter, A. Dhouib, Renew. Energ. **25**(1), 131 (2002).
[10] F. Xue, J. Zhang, W. Hu, W. T. Hsu, A. Han, S. F. Leung, J. K. Huang, Y. Wan, S. Liu, J. Zhang, J. H. He, W. H. Chang, Z. L. Wang, X. Zhang, L. J. Li, ACS Nano. **12**, 4976 (2018).
[11] P. Zhao, Y. Ma, X. Lv, M. Li, B. Huang, Y. Dai, Nano Energy. **51**, 533 (2018).
[12] W. Feng, F. Gao, Y. Hu, M. Dai, H. Liu, L. Wang, P. Hu, ACS Appl. Mater. Inter. **28**(12)**,** 27584 (2018).
[13] Z. Zheng, J. Yao, J. Xiao, G. Yang, ACS Appl. Mater. Inter. **8**(31), 20200 (2018).
[14] H. Zhang, S. Yan, S. Li, S. Su, J. Mater. Sci.: Mater. Electron. **29**(8), 6434 (2018).
[15] C. Julien, E. Hatzikraniotis, A. Chevy, K. Kambas, Mater. Res. Bull. 20(3), 287 (1985).
[16] X. Tao, Y. Gu, Nano Lett. **13**, 3501 (2013).
[17] R. Wang, J. Wan, J. Jia, W. Xue, X. Hu, E. Liu, J. Fan, Mater. Design. **151**, 74 (2018).
[18] D. Wu, A. J. Pak, Y. Liu, Y. Zhou, X. Wu, Y. Zhu , M. Lin, Y. Han, Y. Ren, H. Peng, Y. H. Tsai, G. S. Hwang, K. Lai, Nano Lett. **15**(12), 8136 (2015).
[19] Y. Yan, S. Li, Y. Ou, Y. Ji, Z. Yu, L. Liu, C. Yan, Y. Zhang, Y. Zhao, Electronic Mater. Lett. **10**(6), 1093 (2014).
[20] C. Zhu, H. Shen, H. Liu, X. Lv, Z. Li, Q. Yuan, Chem-Eur. J. **24,** 19060 (2018).
[21] S. Popovic, A. Tonejc, B. Grzeta, B. Celustka, R. Trojko, J. Appl. Crystallogr. **12**(4), 416 (1979).
[22] X. Tan, J. Zhou, Q. Yang, CrystEngComm. **13**(7), 2792 (2011).

[23] J. Ning, G. Xiao, N. Xiao, L. Wang, B. Liu, B. Zou, J. Cryst. Growth. **336**(1), 1 (2011).
[24] D. Wei, Z. Lin, Z. Cui, S. Su, D. Zhang, M. Cao, C. Hu, Chem. Commun. **49**(83), 9609 (2013).
[25] Y. Liu, M. A. Summers, C. Edder, J. M. J. Fréchet, M. D. McGehee, Adv. Mater. **17**(24), 2960 (2005).
[26] J. Wang, Y. Wang, F. Cao, Y. Guo, L. Wan, J. Am. Chem. Soc. **132**(35), 12218 (2010).
[27] S. Zhou, X. Tao, Y. Gu, J. Phys. Chem. C. **120**(9), 4753 (2016).
[28] J. Zhou, Q. Zeng, D. Lv, L. Sun, L. Niu, W. Fu, F. Liu, Z. Shen, C. Jin, Z. Liu, Nano Lett. **15**(10), 6400 (2015).
[29] N. Balakrishnan, C. R. Staddon, E. F. Smith, J. Stec, D. Gay, G. W. Mudd, O. Makarovsky, Z. R. Kudrynskyi, Z. D. Kovalyuk, L. Eaves, A. Patanè, P. H. Beton, 2D Mater. **3**(2), 025030 (2016).
[30] X. G. Peng, Adv. Mater. **15**(5), 459 (2010).
[31] R. López, R. Gómez, J. Sol-Gel Sci. Techn. **61**(1), 1 (2011).
[32] W. Li, F. P. Sabino, F. Crasto de Lima, T. Wang, R. H. Miwa, A. Janotti, Phys. Rev. B. **98**(16), 165134 (2018).